NASA CONTRACTOR
REPORT

Report No. 61283

PLUME CHARACTERISTICS OF THE SATURN CLUSTER MODEL

By D. O. Barnett

Nortronics-Huntsville
6205 Technology Drive
Huntsville, Alabama

December 23, 1968

Interim Report

Prepared for

NASA-George C. Marshall Space Flight Center
Marshall Space Flight Center, Alabama 35812

TECHNICAL REPORT STANDARD TITLE PAGE

1. Report No.	2. Government Accession No.	3. Recipient's Catalog No.
NASA CR-61283		

4. Title and Subtitle	5. Report Date
PLUME CHARACTERISTICS OF THE SATURN CLUSTER MODEL	Dec 23, 1968
	6. Performing Organization Code

7. Author(s)	8. Performing Organization Report No.
D. O. Barnett	M 79-8-472

9. Performing Organization Name and Address	10. Work Unit No.
Nortronics-Huntsville 6205 Technology Drive Huntsville, Alabama	933-50-19-9000
	11. Contract or Grant No. NAS8-20082
	13. Type of Report and Period Covered
12. Sponsoring Agency Name and Address NASA-Marshall Space Flight Center Marshall Space Flight Center, Alabama 35812	14. Sponsoring Agency Code

15. Supplementary Notes

This work was done under Northrop Mission Support Contract NAS8-20082, Schedule Order 109.

16. Abstract

This report presents results on one phase of a program to determine acoustic and hydromechanical loads at the base of Saturn configured vehicles. Data are presented on pitot pressure distributions across clusters of one to four jets exhausting at stagnation-to-ambient pressure ratios of 35 to 105 atmospheres. The data are compared with results to a method of characteristics solution for the flow field. An empirical correlation is given for the growth of the shear region of the plumes near the nozzle exit plane. It is seen that shear layer thickness varies directly with axial location and inversely with stagnation pressure.

17. Key Words	18. Distribution Statement
Plume characteristics, pitot pressure distributions, cluster jets, plume flow fields	Public Release

19. Security Classif. (of this report)	20. Security Classif. (of this page)	21. No. of Pages	22. Price
Uncl	Uncl	32	

NORTHROP NORTRONICS A Division of Northrop Corporation

Nortronics Huntsville
6025 Technology Drive, Huntsville, Alabama 35805
Telephone (205) 837-0580

PLUME CHARACTERISTICS OF THE SATURN CLUSTER MODEL

BY

D. O. Barnett

SUMMARY

This report presents results on one phase of a program to determine acoustic and hydromechanical loads at the base of Saturn configured vehicles. Data are presented on pitot pressure distributions across clusters of one to four jets exhausting at stagnation-to-ambient pressure ratios of 35 to 105 atmospheres. The data are compared to results of a method of characteristics solution for the flow field. An empirical correlation is given for the growth of the shear region of the plumes near the nozzle exit plane. It is seen that shear layer thickness varies directly with axial location and inversely with stagnation pressure.

I. INTRODUCTION

The total pressure distribution across the plumes of the Saturn Cluster Model was studied experimentally in Tests TAJF-010 and -011. In these investigations radial pitot traverses were made at several axial locations for chamber stagnation pressures of 500, 900, and 1500 psig. Configurations studied included combinations of one to four nozzles blowing. The Saturn configuration was excluded from these tests since, for measurements taken in a single plane, the plume intersection regions were adequately defined by less than five jets exhausting.

These investigations were primarily conducted to define the location of the free-shear layers for subsequent Crossed-Beam Tests. A secondary objective,

however, was the qualitative understanding of these flow fields as an aid in studies of recirculatory and acoustic phenomena induced by clustered jets. This memorandum, thus, presents data taken in the investigations, the thickness of the combined shock-shear layer, and discusses the possible distribution of velocities across the jets for different test conditions, configurations and axial locations.

II. EXPERIMENTAL CONSIDERATIONS

The Saturn Cluster Model consists of an adapter section for mating with the Cold Flow Duct, a baseplate, and five nozzles arranged as shown in Figure 1. The center nozzle is removable and may be replaced by an adapter plate to simulate a symmetric four-jet cluster. The nozzles are capable, moreover, of being internally closed to allow the jets to exhaust in any combination from one to five.

Design of the nozzles was made on the basis of plume contour at a chamber pressure of $P_0^{\dagger}$ = 1500 psig. The specific criterion used was the matching of S-II Stage plumes at the "max q" condition. A suitable nozzle geometry for such matching with ambient temperature air was obtained by a method of characteristics solution and is shown in Figure 2.

Pitot data were taken by either a 20-tube pitot rake (TAJF-010) or a traversing-single probe (TAJF-011). The probes were mounted on a probe cart which could be moved along rails to each subsequent axial location. Probe location with respect to the model referenced coordinate system of Figure 3 was determined to within 0.01 inch (ref. 1). Measurements were made only in the Z=0 plane. The pressure recording system as well as details on the facility and test procedures are given in reference 2.

III. DESCRIPTION OF PLUME FLOW FIELD

Before examining the pitot data, it is useful to discuss the characteristics of the plume flow field. Figure 4 is a Schlieren photograph of a single plume exhausting from a stagnation pressure of 900 psig. (All photographic data presented were obtained in Test TAJF-009 (ref. 3). The nozzle flow is underexpanded and expands rapidly downstream of the nozzle exit plane. Static pressures in the plume core are far below the ambient pressure of 14.4 psia (nominal). This

---

†Complete nomenclature given in section VII.

pressure differential is accommodated by the shock system seen in the picture. The inner boundary shock originates within the nozzle and is the stronger shock. A secondary lip shock is necessary to complete the pressure rise to ambient. The viscous shear layer apparently lies mostly outside the lip shock.

The additional complexity introduced in the jet interaction regions is exemplified by Figure 5. It is seen that in the vicinity of an intersection point the shock formed by the plume impingement coalesces with the boundary shocks to form a stronger interaction shock. Increasing the number of jets blowing increases the number of interactions as in Figure 6, as well as creating regions where interactions between three or even four plumes occur simultaneously.

Conditions further downstream in the flow are shown in the shadowgraph of Figure 7. At a location dictated by the stagnation to ambient pressure ratio, a Mach disk forms in the individual plumes. For the two-jet case shown, this normal shock intersects the interaction shock resulting in a secondary interaction shock and formation of an additional Mach disk. The extension of this process to additional plumes may readily be imagined.

IV. PITOT PRESSURE PROFILES

Figure 8 presents the distribution of pitot pressure ratios, P_0^*/P_0, across a single plume at several axial locations. The individual parts of the figure correspond to stagnation-to-ambient pressure ratios, P_0/P_a, of 105.2, 63.5, and 35.7, i.e., nominal stagnation pressures of 1500, 900, and 500 psig, respectively.

Two striking characteristics of the data are (1) the higher pressure recoveries in the center of the plume at low X/D ratios, and (2) the sharp rise in pressure recovery near the edge of the plume. The first phenomena, as will be shown later, is due to lower velocities and Mach numbers along the nozzle centerline than further out in the flow. The latter effect is clearly due to the plume interior shock. This conclusion was reached after repeated experimental measurements showed the maximum recovery rise occurs immediately outside the interior shock. However, attempts to analyze this affect one-dimensionally were unsuccessful, although the apparent reason for the rise is an increase in pressure recovery

across an oblique-normal shock system. This point, too, will be discussed later.

Figure 9 shows the pitot profiles for a two-jet configuration. The characteristics of the data are similar to those for a single plume except additional departures from the data trend are obtained in the vicinity of the interaction shocks arising from plume impingement. Additional data are presented in Figures 10 and 11 for the three- and four-jet configurations. These data are of limited interest, however, since probing in a single plane (Z=0) caused many of the interaction effects to be missed.

V. DISCUSSION OF RESULTS

To form a basis for comparison with results of the tests, the plume flow field for a single nozzle was analyzed using the method of characteristics program of reference 4. Figure 12 shows the inner shock and plume boundary predicted by the method of characteristics for a stagnation pressure of 1500 psig. Agreement of the theoretical results with the actual location of the interior shock is excellent. The plume boundary predicted by the characteristics solution coincides, moreover, with the location of the lip shock. This tends to further substantiate the conclusion given earlier that the shear layer lies outside the lip shock.

Figure 13 gives the comparison of theoretical and experimental pitot pressures across the plume at two axial locations. Agreement is good in the core of the jet but the results diverge near the interior shock. Figure 14 compares the Mach number variation across the plume as obtained from the characteristics solution to one-dimensional flow results computed from the pitot data. Once again agreement is good in the core but the divergence in results near the interior shock has been amplified.

These comparisons point out the extreme difficulty in using pitot data to estimate velocity variations through the shock-shear region of an underexpanded plume. In the potential core the use of one-dimensional results gives an accurate value for Mach number and velocity of the flow. In the subsonic portion, along the outer edge of the plume, an accurate estimate should also be possible using the measured pitot pressure and the anticipated result of static pressure equal to ambient pressure. Between these extremes no such obvious procedure is possible.

For example, outside the interior shock the flow remains supersonic but the stagnation pressure ahead of the pitot-tube-bow shock is unknown from purely experimental considerations. An iterative one-dimensional approach to this problem was attempted. By considering flow across an oblique shock (corresponding to the interior shock) and a normal shock (pitot-tube-bow shock), it was possible to iterate on the shock angle for a known approach Mach number to obtain a match with the pitot data. This method was applied to the present data but the match sought was not obtained for the apparent Mach number ahead of the oblique shock. A second difficulty arises in considering the method by which static pressures must attain equilibrium with the ambient pressure. The characteristics solution, which is qualitatively correct, shows that static pressures are substantially below ambient after the interior shock. This suggests an additional mechanism must be present to accommodate the static pressure rise. The lip shock seen in Figure 11 furnishes such a mechanism near the nozzle-exit plane. It appears to vanish further downstream, however, suggesting some other process such as liquifaction of flow constituents may complete the pressure rise process.

In view of this complex situation, consideration was given to an empirical estimate of velocity variation across the shock-shear zone. Abromovich, reference 5, presents a correlation which agrees well with data taken in supersonic jet-shear layers. Consider the coordinate system shown in Figure 15. If the velocity at y=0 is defined as U_0, then the velocity variation may be given in terms of the similarity variable $\eta = y/\delta(x)$ by

$$\frac{U}{U_0} = 1 - [1 - (1-\eta)^{3/2}]^2$$

Velocity profiles across a single nozzle using this correlation in conjunction with isentropic flow relations in the potential core are given in Figures 16 and 17 for stagnation pressures of 500, and 1500 psig, respectively. The flow near the nozzle-exit plane of this nozzle is much faster along the edge of the potential region than along the centerline. Such differences, however, tend to vanish within 1 to 2 diameters of the exit. This explains the substantially higher pressure recoveries obtained in the jet core near the nozzle exit.

The extent of the shock-shear region near the exit plane more readily lends itself to interpretation. Figure 18 shows that the thickness of this region, measured normal to the nozzle centerline, varies directly with the axial distance, X/D, and inversely to the stagnation-ambient pressure ratio, P_0/P_a. This variation is linear in terms of the scaling parameter

$$\phi = \left(\frac{X}{D}\right)^{.565} \left(\frac{P_0}{P_a}\right)^{-.435}$$

and may be expressed as

$$\frac{\delta}{D} = 0.02 + 1.44\phi$$

VI. CONCLUSIONS

The pitot data taken in Tests TAJF-010 and -011 give an accurate indication of the extent of the shock-shear region of the Saturn Cluster Model as was originally intended. The use of such data to determine other characteristics of the flow such as shear-layer thickness (per se), velocity distribution across the shear layer and other derivable quantities is of doubtful validity due to the complex nature of the multiple boundary shocks in the jets. Although discussion has been limited to the outer edge of the plumes and near the nozzle exit planes, the same limitations occur in the interior-shock regions of intersecting jets and further downstream in the flow.

VII. NOMENCLATURE

D	Nozzle Exit Diameter - inches
M	Mach Number
P_a	Ambient Pressure - psia
P_o	Chamber Stagnation Pressure - psi
P_o^*/P_o	Pitot Pressure Ratio
q	Dynamic Pressure - psia
r/D	Transverse Measurement from Nozzle Centerline - inches
T_o	Chamber Stagnation Temperature - °R
U	Velocity - ft/sec
U_o	Velocity at y=0 in Shear Layer Coordinate System - ft/sec
x,y	Shear Layer Coordinates (Figure 15)
X,Y,Z	Model Referenced Coordinates (Figure 3)
δ	Shear Layer Thickness - inches
η	Dimensionless Shear Layer Location
ϕ	Dimensionless Scaling Parameter Defined on Page 6

Subscripts

y	Measured at y
r	Measured at r

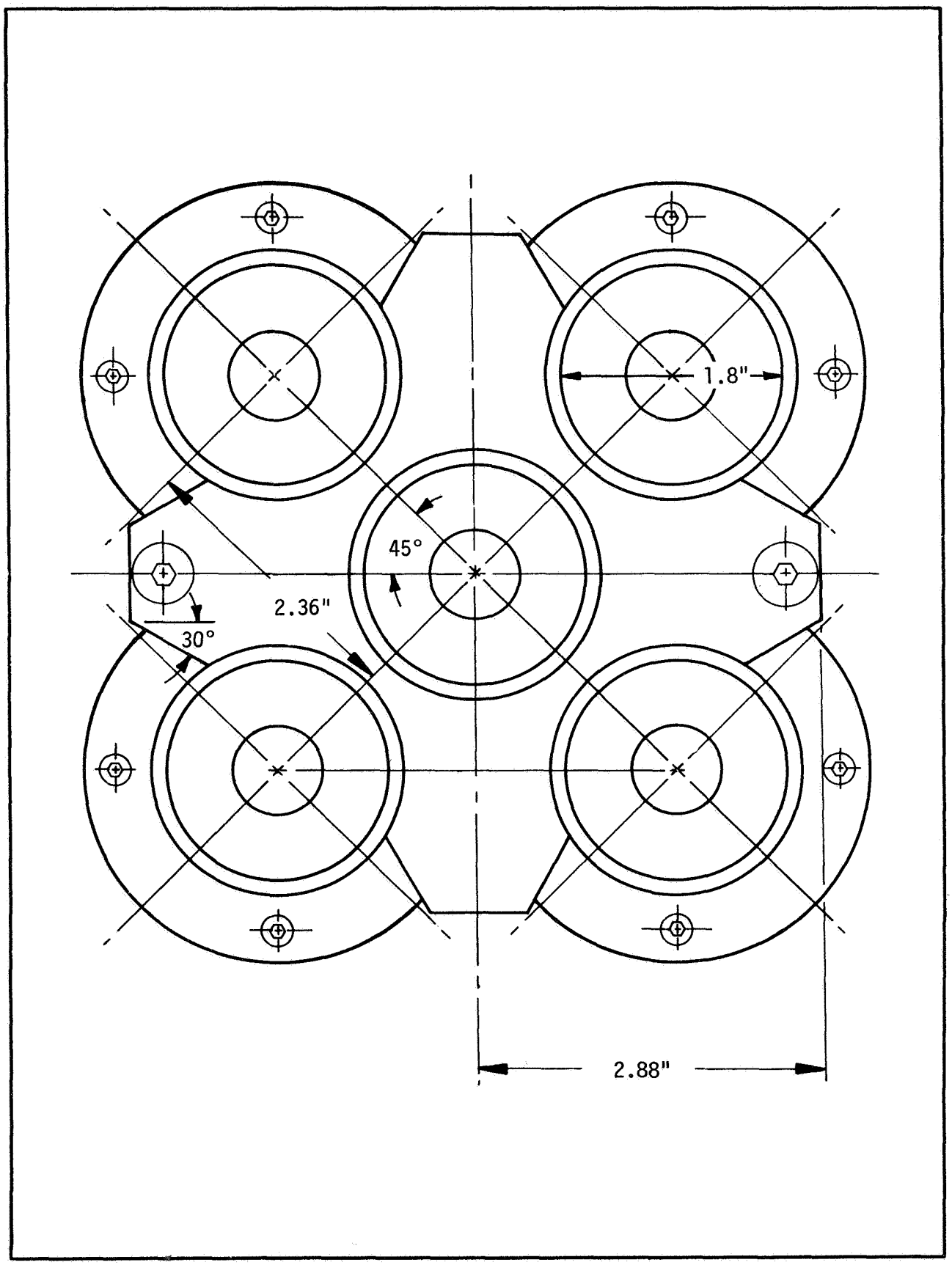

Figure 1. SATURN CLUSTER MODEL BASE GEOMETRY

Internal Contour	
X	Y
0	.9000
.0210	.8778
.0417	.8556
.0521	.8443
.0790	.8147
.0813	.8121
.0984	.7927
.1154	.7733
.1322	.7538
.1488	.7341
.1652	.7143
.1813	.6943
.1976	.6741
.2136	.6537
.2296	.6330
.2454	.6119
.2612	.5906
.2768	.5688
.2924	.5467
.3080	.5240
.3234	.5009
.3388	.4772
.3541	.4528
.3694	.4277
.3845	.4018
.3995	.3750
.4495	.3755
.4995	.3770
.5495	.3793
.5995	.3827
.6495	.3870
.6995	.3922
.7495	.3985
.7995	.4057
.8495	.4139
.8995	.4231
.9995	.4445
1.0995	.4701
1.1995	.4999
1.2995	.5342
1.3995	.5682
1.4995	.5972
1.5995	.6213
1.6995	.6404
1.7995	.6545
1.8995	.6636
2.0327	.6680

External Contour	
X	Y
0	.900
.180	.893
.360	.866
.540	.815
..720	.756
.880	.668
.911	.869
1.012	.970
1.112	1.021
1.213	1.048
1.314	1.049
1.350	1.051

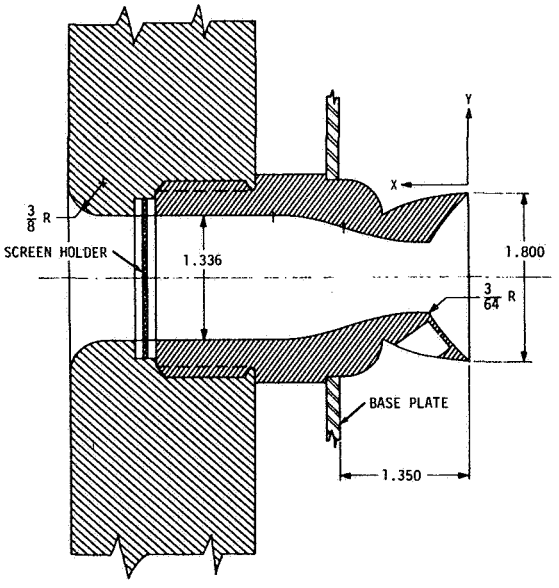

Figure 2. SATURN CLUSTER MODEL NOZZLE GEOMETRY

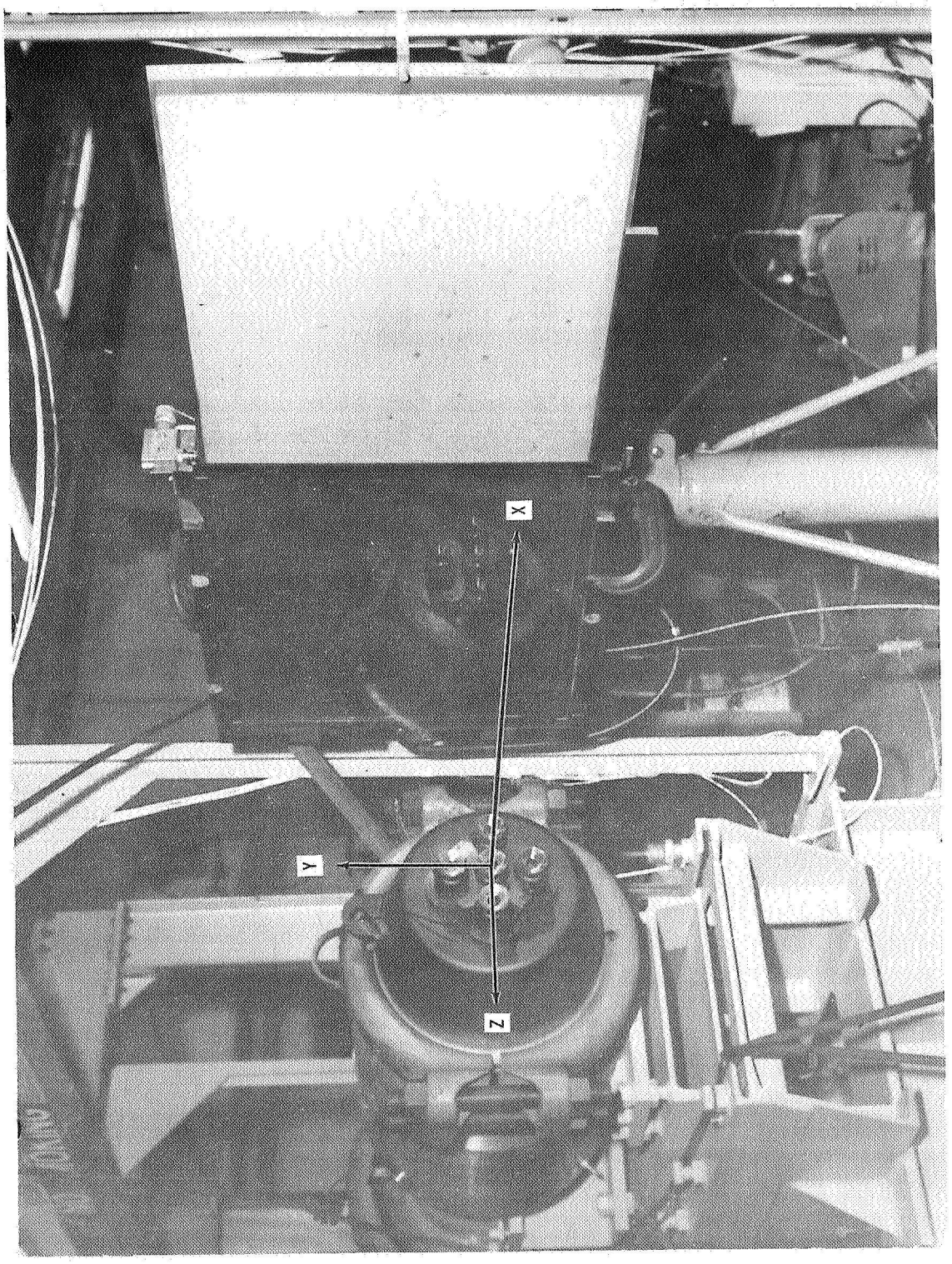

Figure 3. MODEL REFERENCED COORDINATE SYSTEM

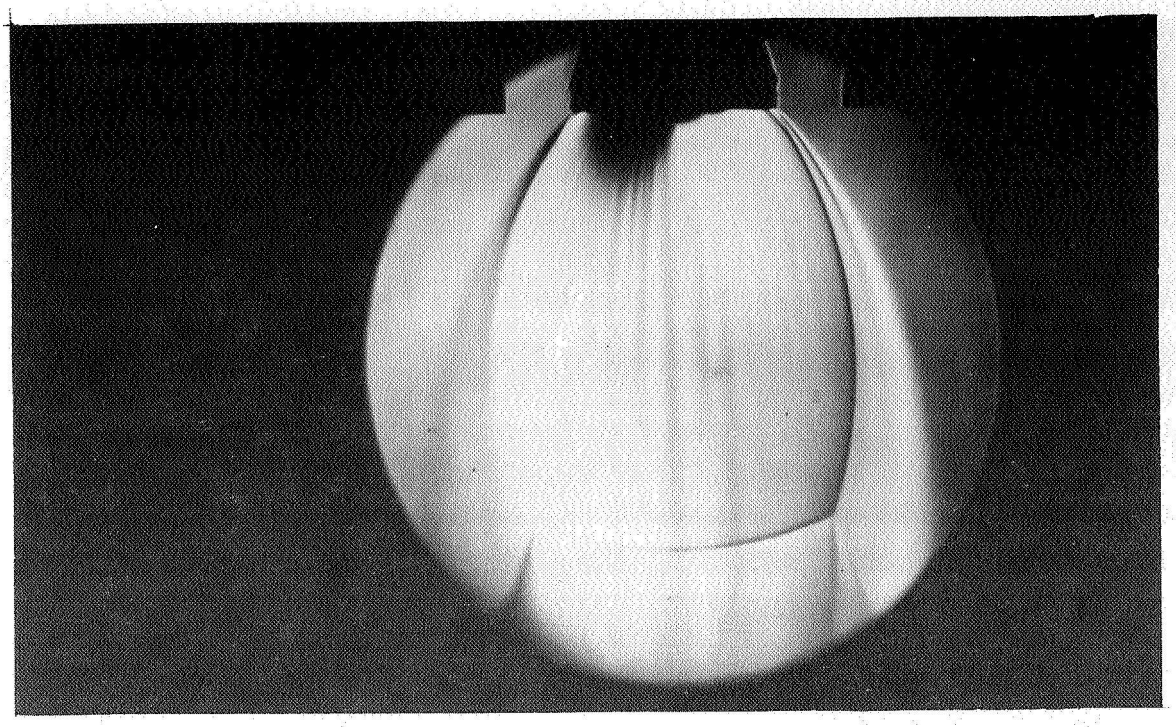

Figure 4. A SINGLE NOZZLE EXHAUSTING FROM A STAGNATION PRESSURE OF 900 PSIG

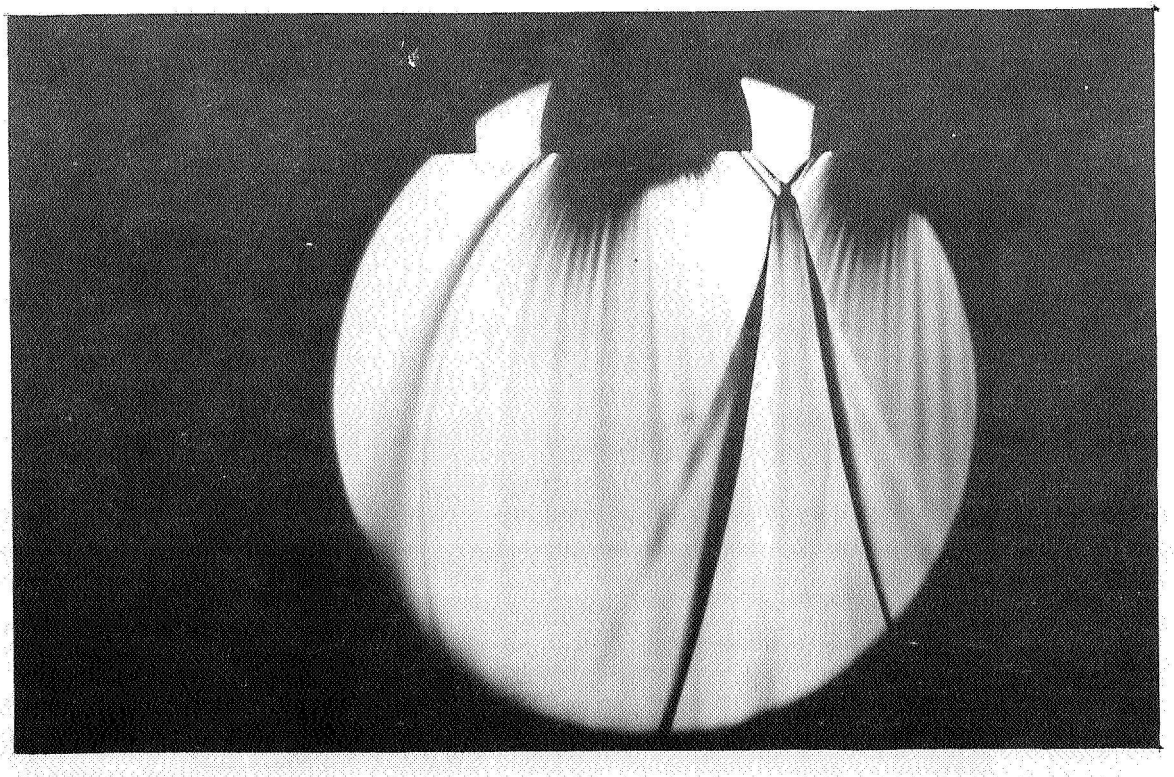

Figure 5. JET INTERACTION REGION FOR A TWO-JET CONFIGURATION (P_o = 1500 PSIG)

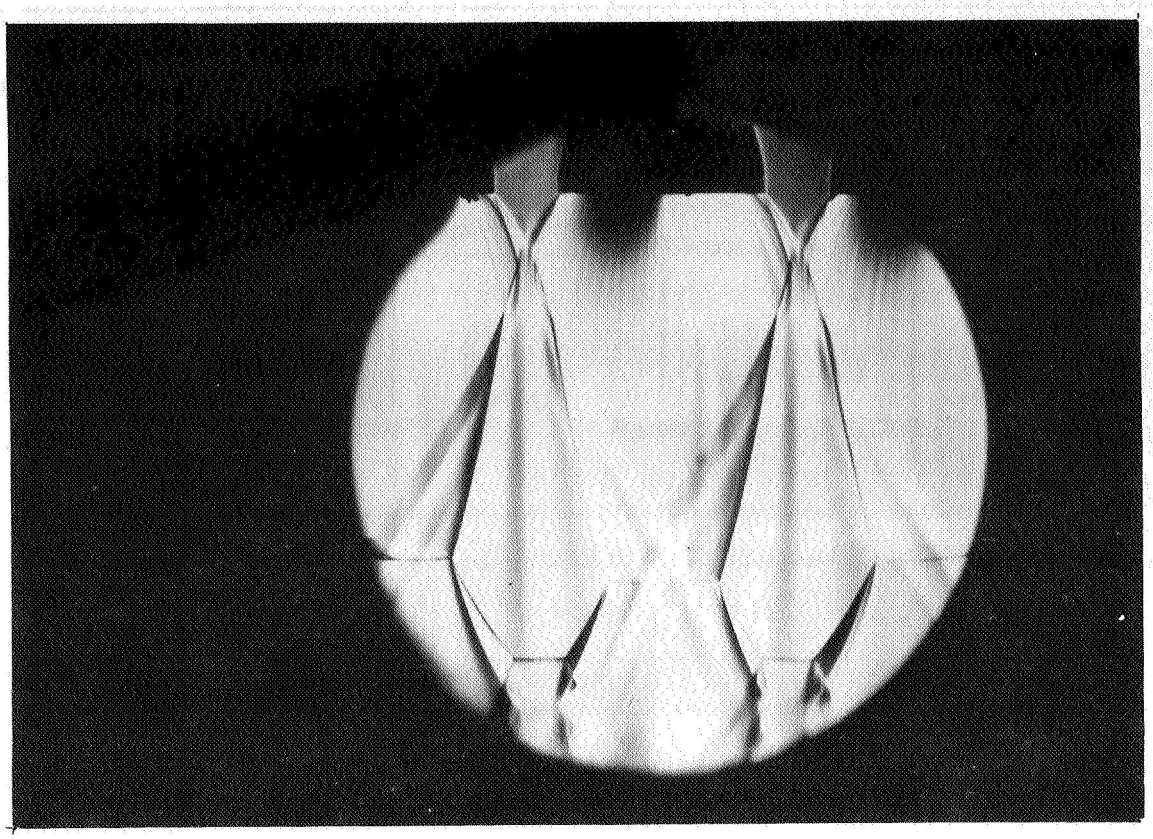

Figure 6. MULTIPLE JET INTERACTIONS FOR SATURN CONFIGURED CLUSTER (P_o = 600 PSIG)

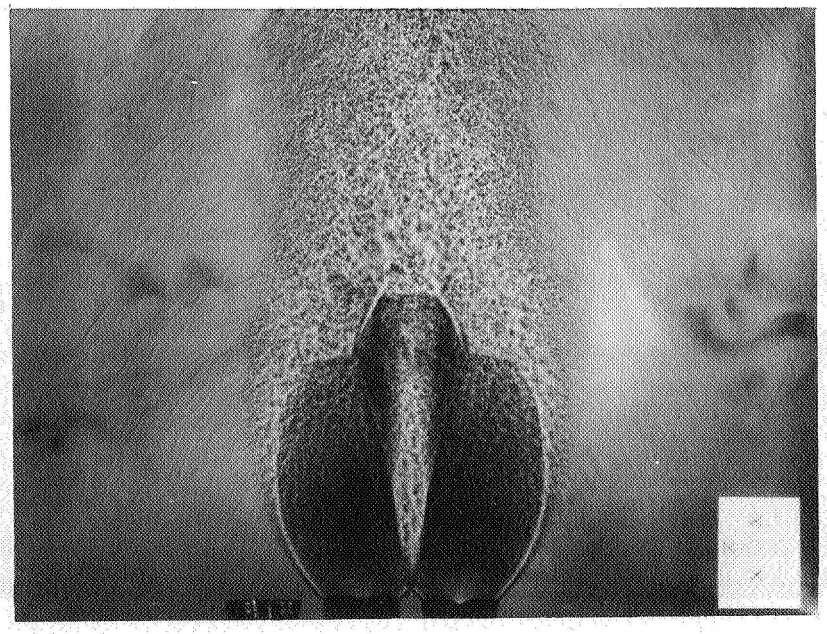

Figure 7. SHADOWGRAPH OF TWO JET FLOW FIELD (P_o = 1500 PSIG)

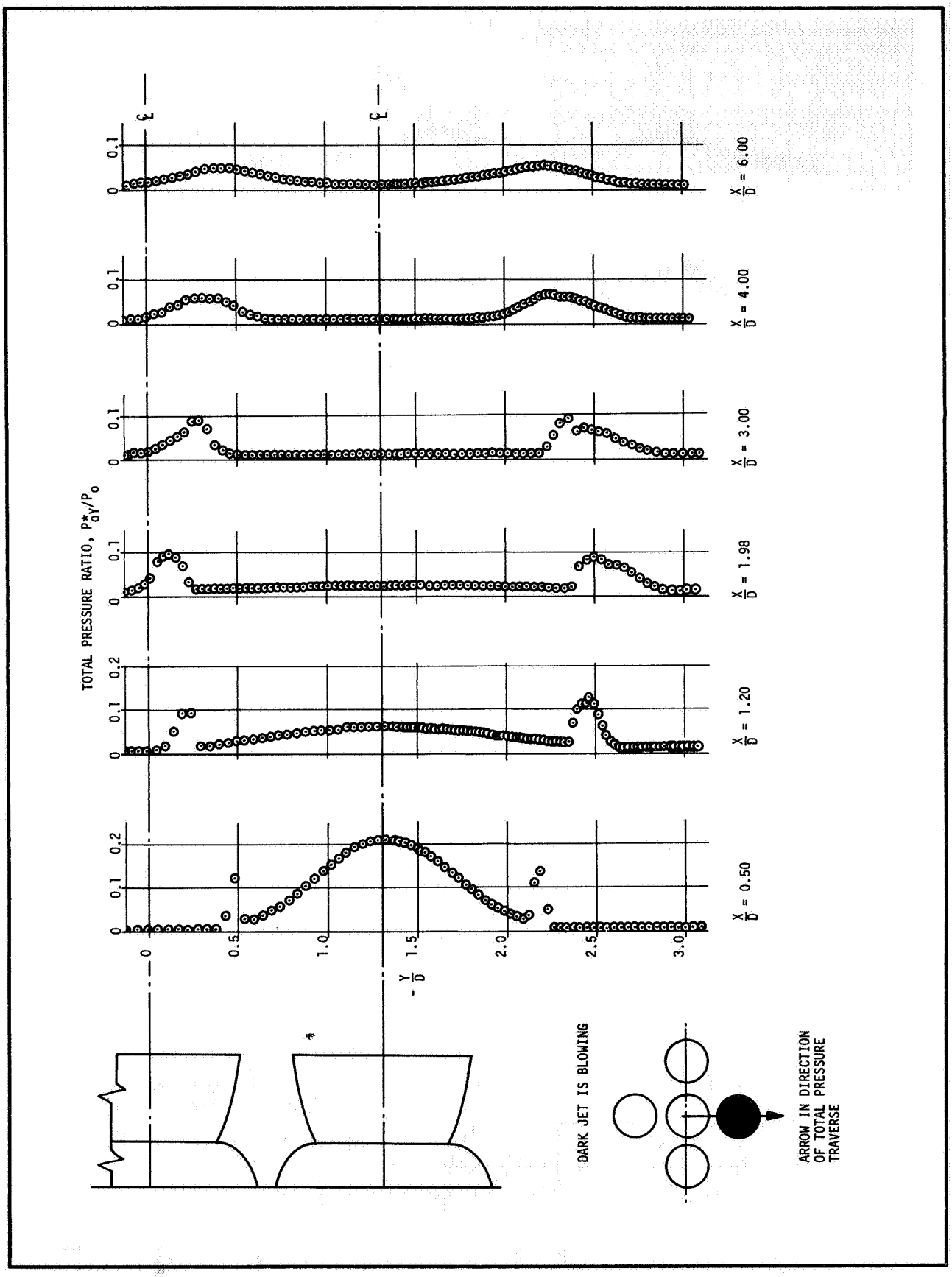

Figure 8a. PLUME TOTAL PRESSURE RATIOS FOR SINGLE JET IN TAJF COLD FLOW
P_o/P_a = 105.2, NOMINAL T_o = 520°R

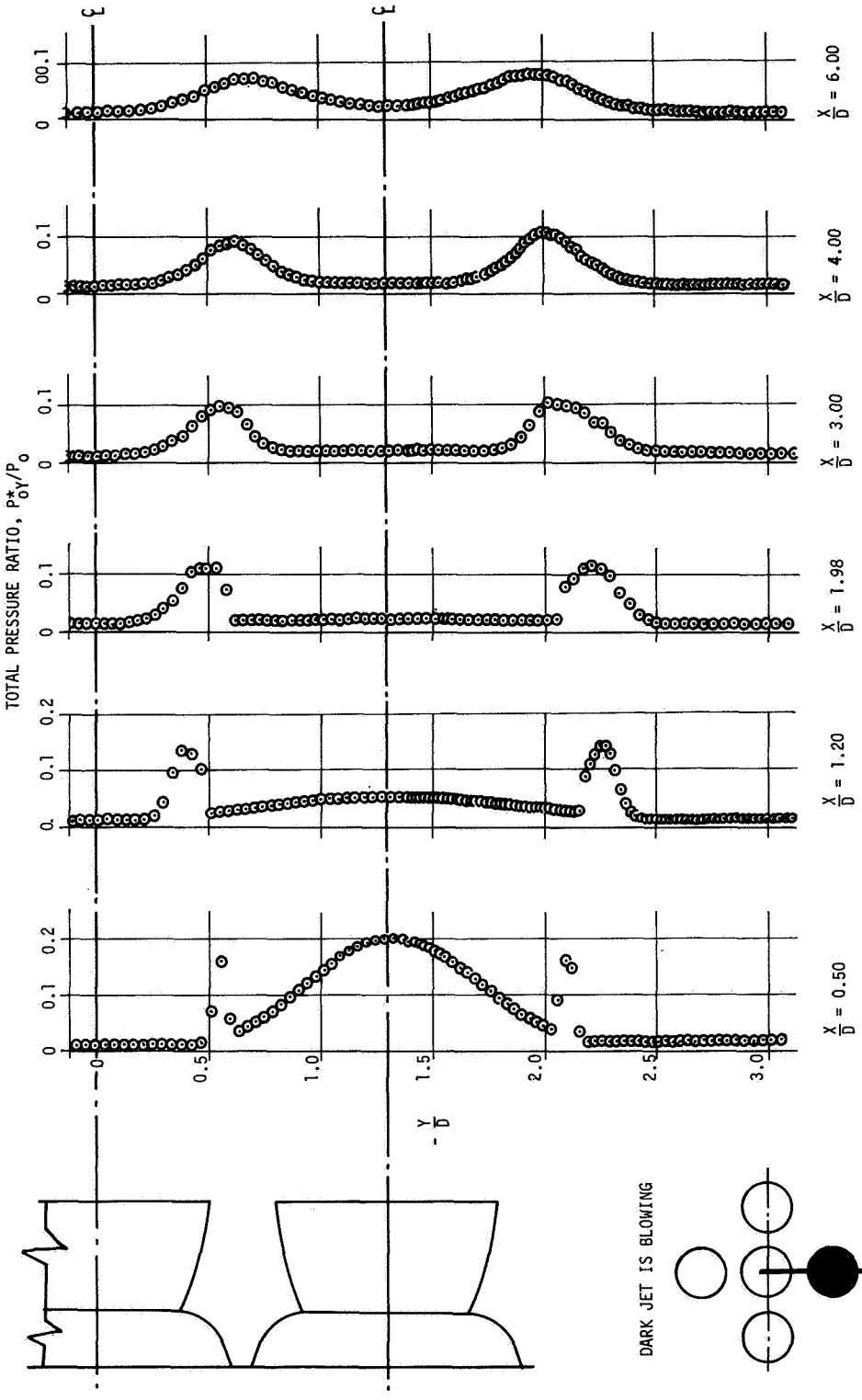

Figure 8b. PLUME TOTAL PRESSURE RATIOS FOR SINGLE JET IN TAJF COLD FLOW
P_o/P_a = 63.5, NOMINAL T_o = 510°R

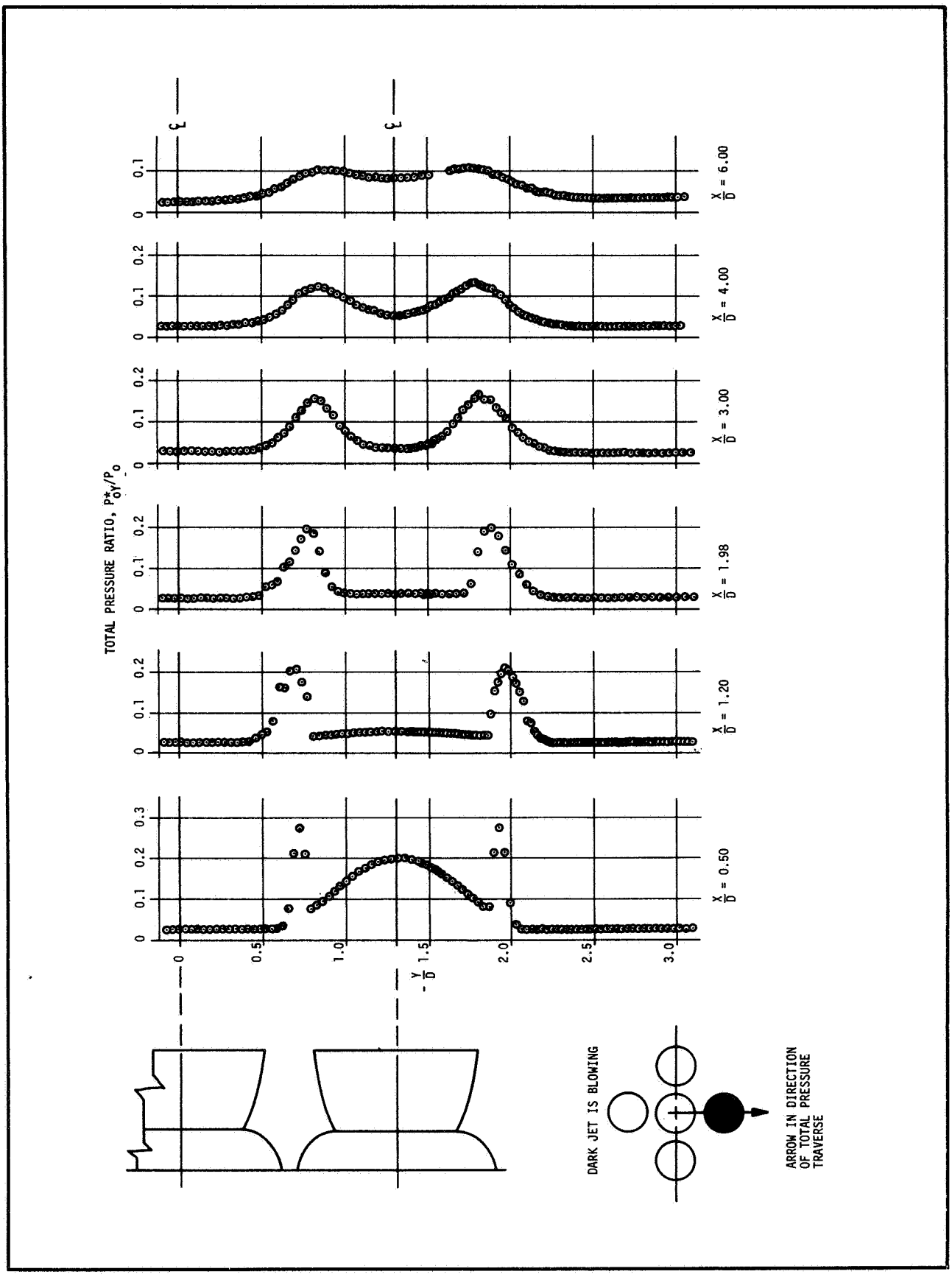

Figure 8c. PLUME TOTAL PRESSURE RATIOS FOR SINGLE JET IN TAJF COLD FLOW
P_o/P_a = 37.5, NOMINAL T_o = 500°R

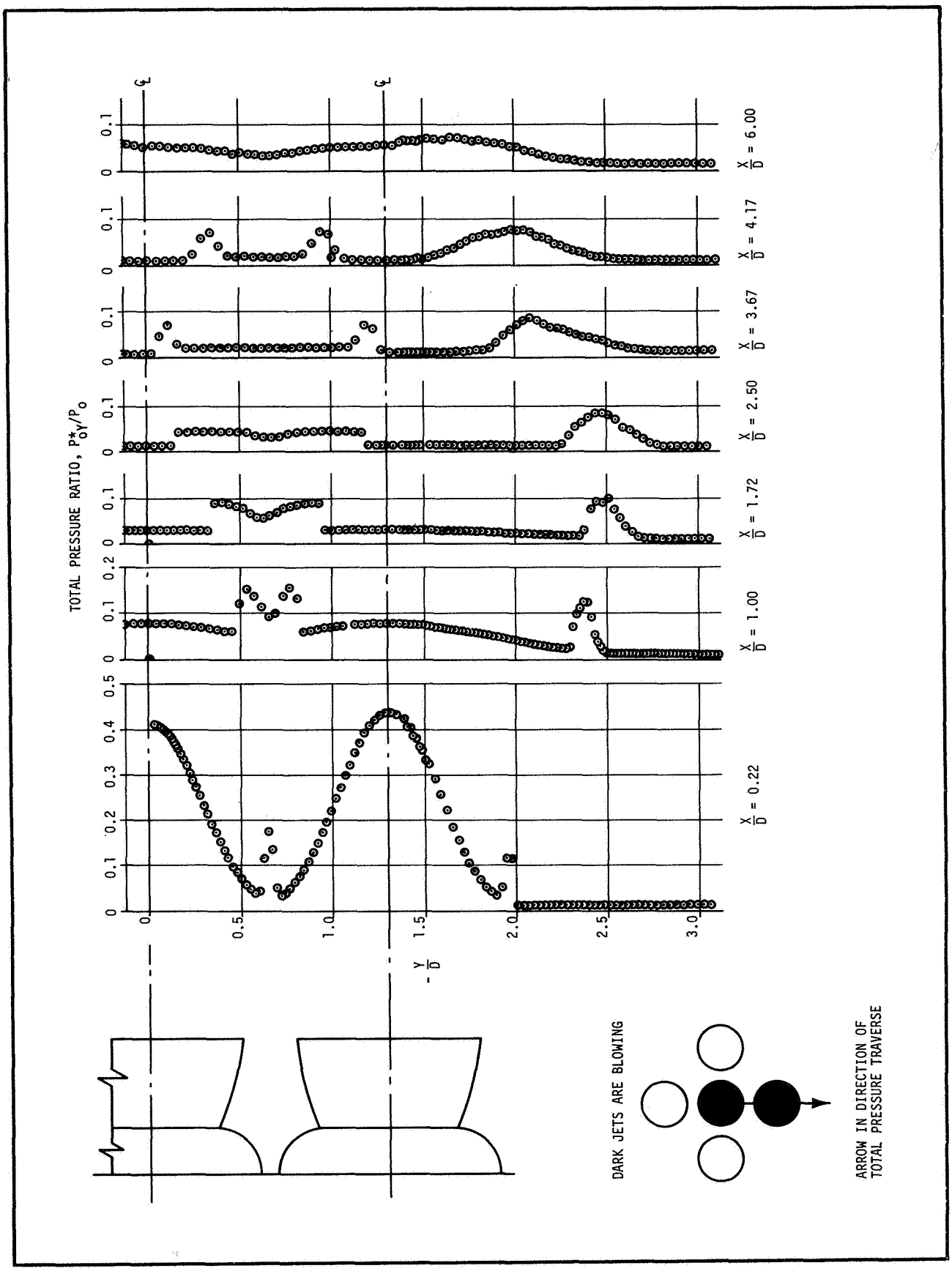

Figure 9a. PLUME TOTAL PRESSURE RATIOS FOR TWO JET CLUSTER IN TAJF COLD FLOW
P_o/P_a = 105.2, NOMINAL T_o = 520°R

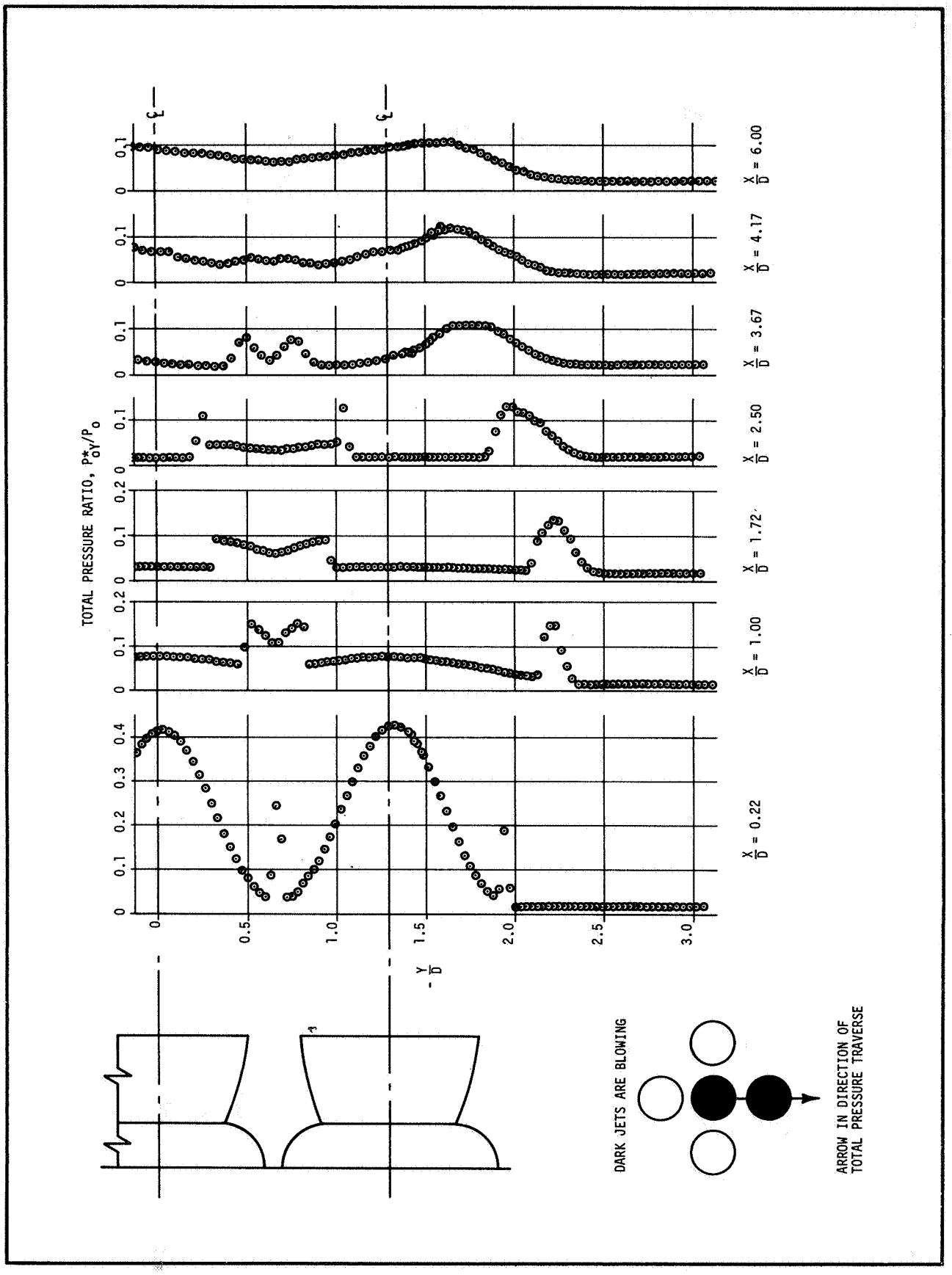

Figure 9b. PLUME TOTAL PRESSURE RATIOS FOR TWO JET CLUSTER IN TAJF COLD FLOW
P_o/P_a = 63.5, NOMINAL T_o = 510°R

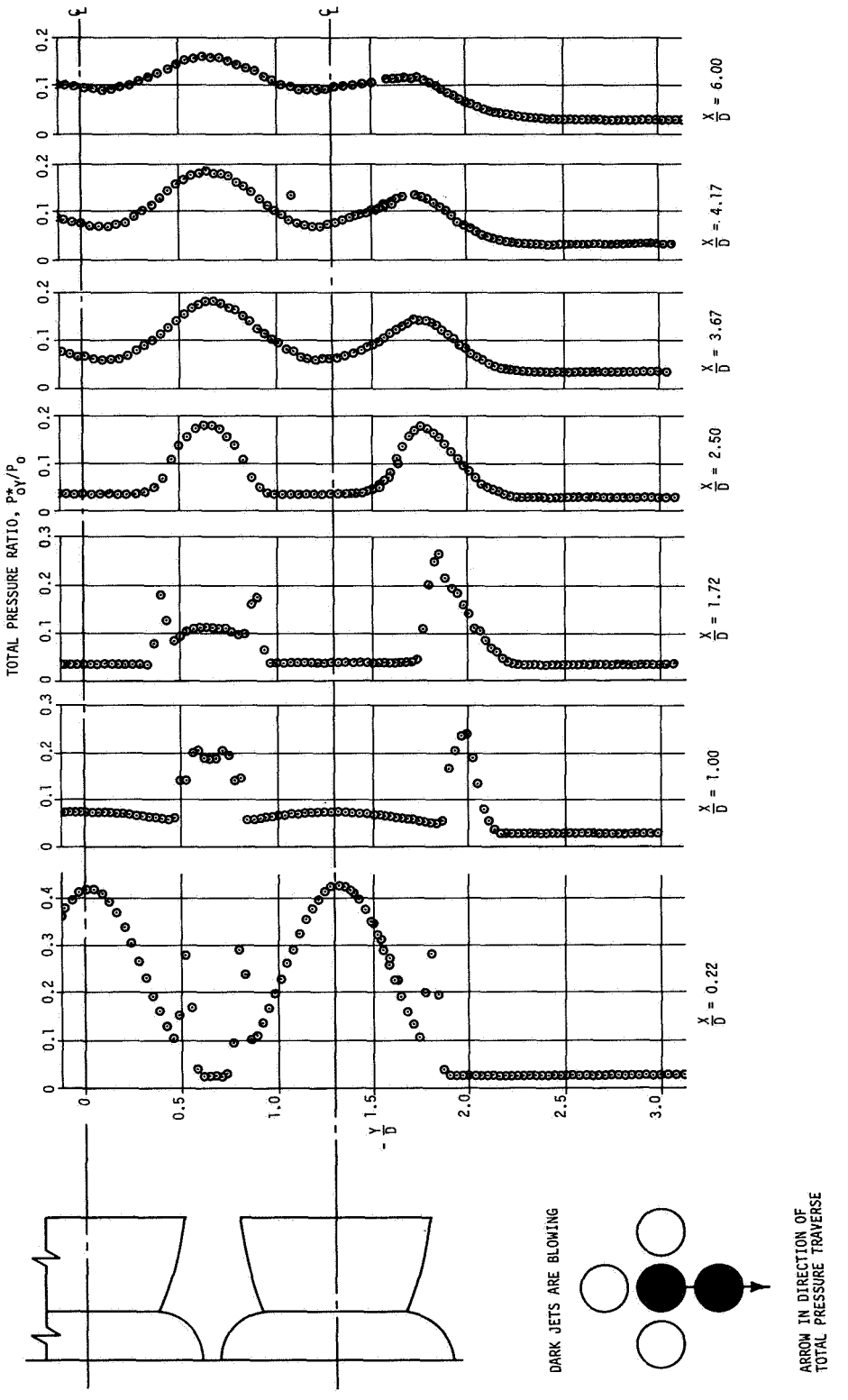

Figure 9c. PLUME TOTAL PRESSURE RATIOS FOR TWO JET CLUSTER IN TAJF COLD FLOW
P_o/P_a = 35.7, NOMINAL T_o = 500°R

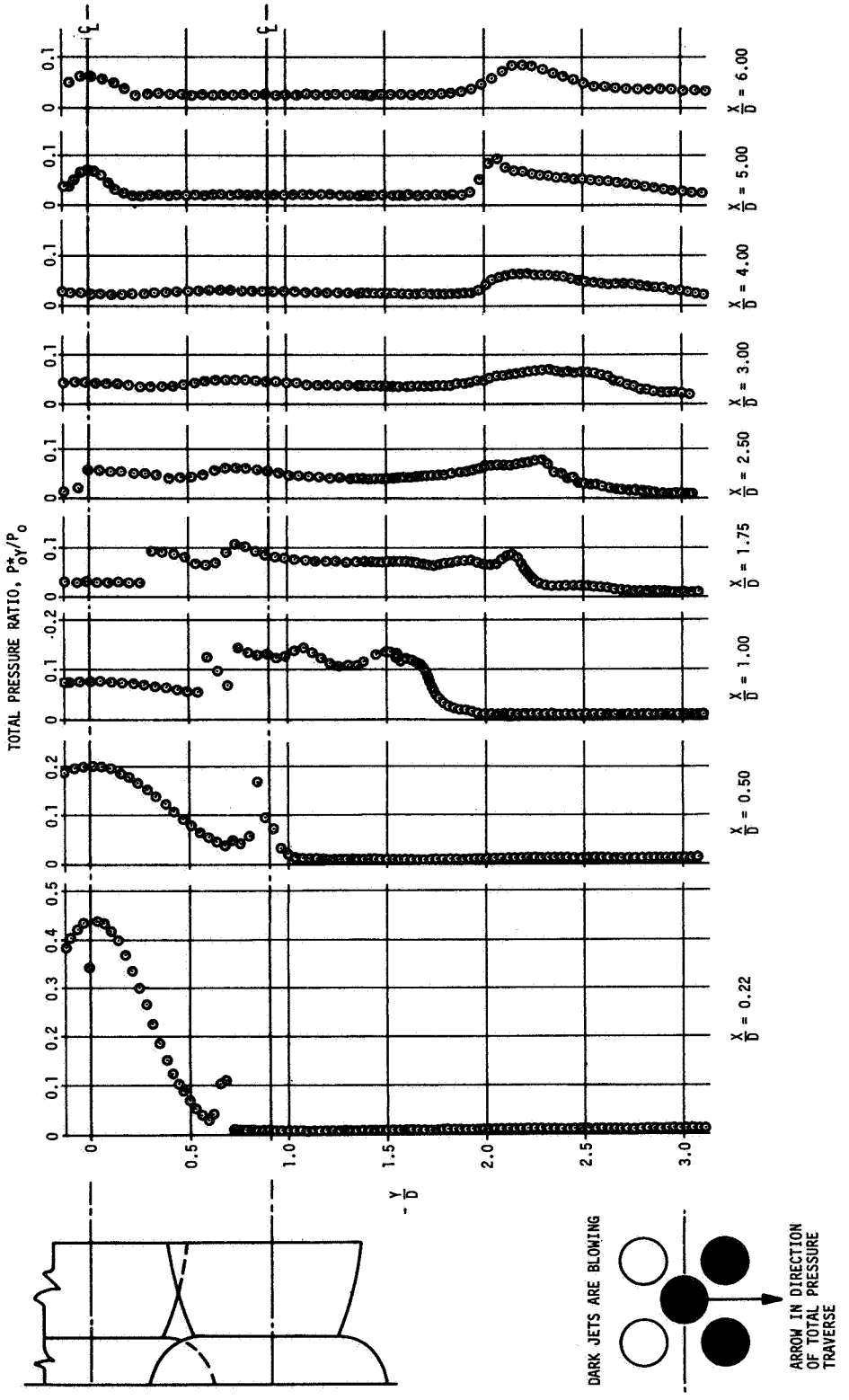

Figure 10a. PLUME TOTAL PRESSURE RATIOS FOR THREE JET CLUSTER IN TAJF COLD FLOW
P_o/P_a = 105.2, NOMINAL T_o = 520°R

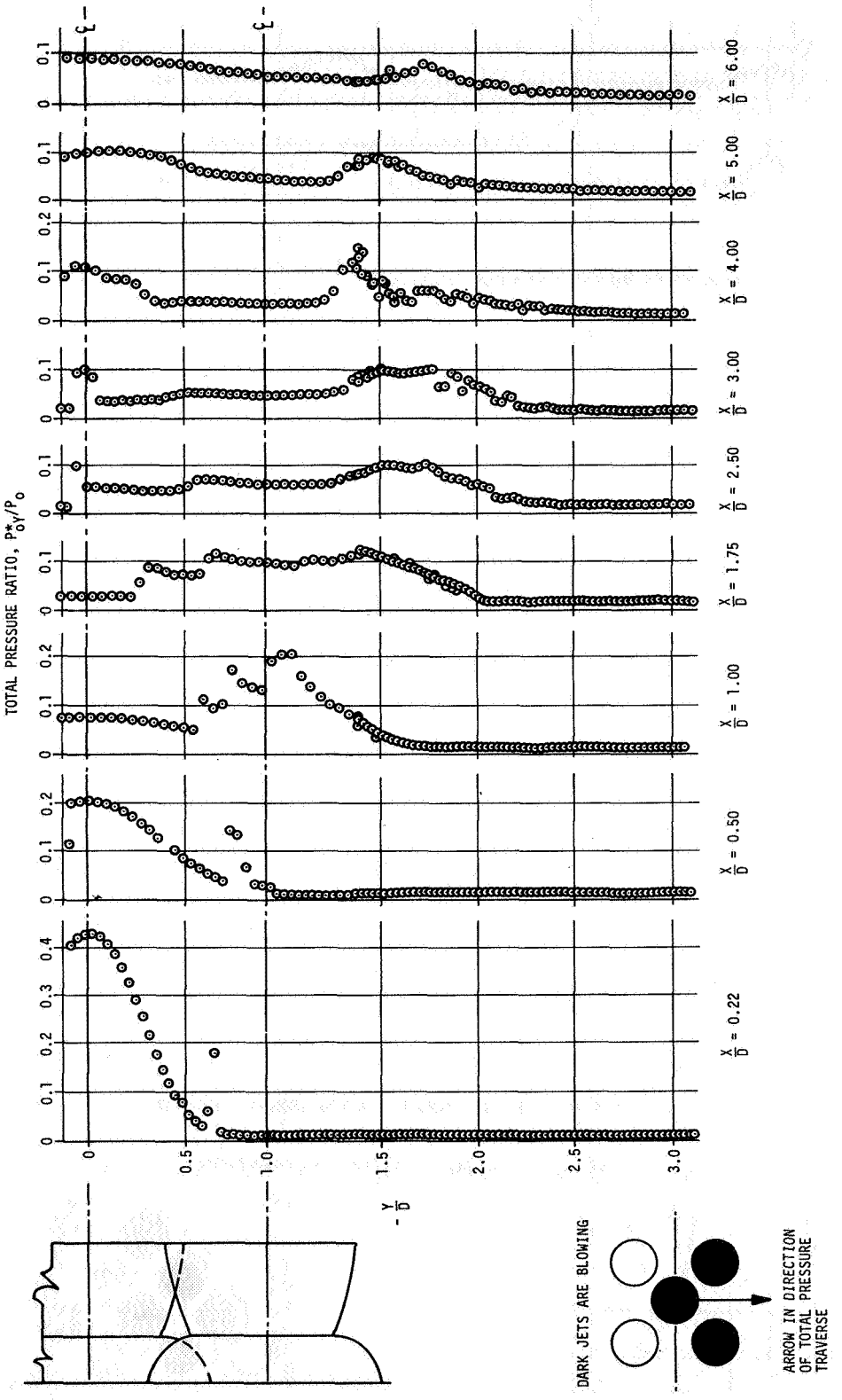

Figure 10b. PLUME TOTAL PRESSURE RATIOS FOR THREE JET CLUSTER IN TAJF COLD FLOW
P_o/P_a = 63.5, NOMINAL T_o = 510°R

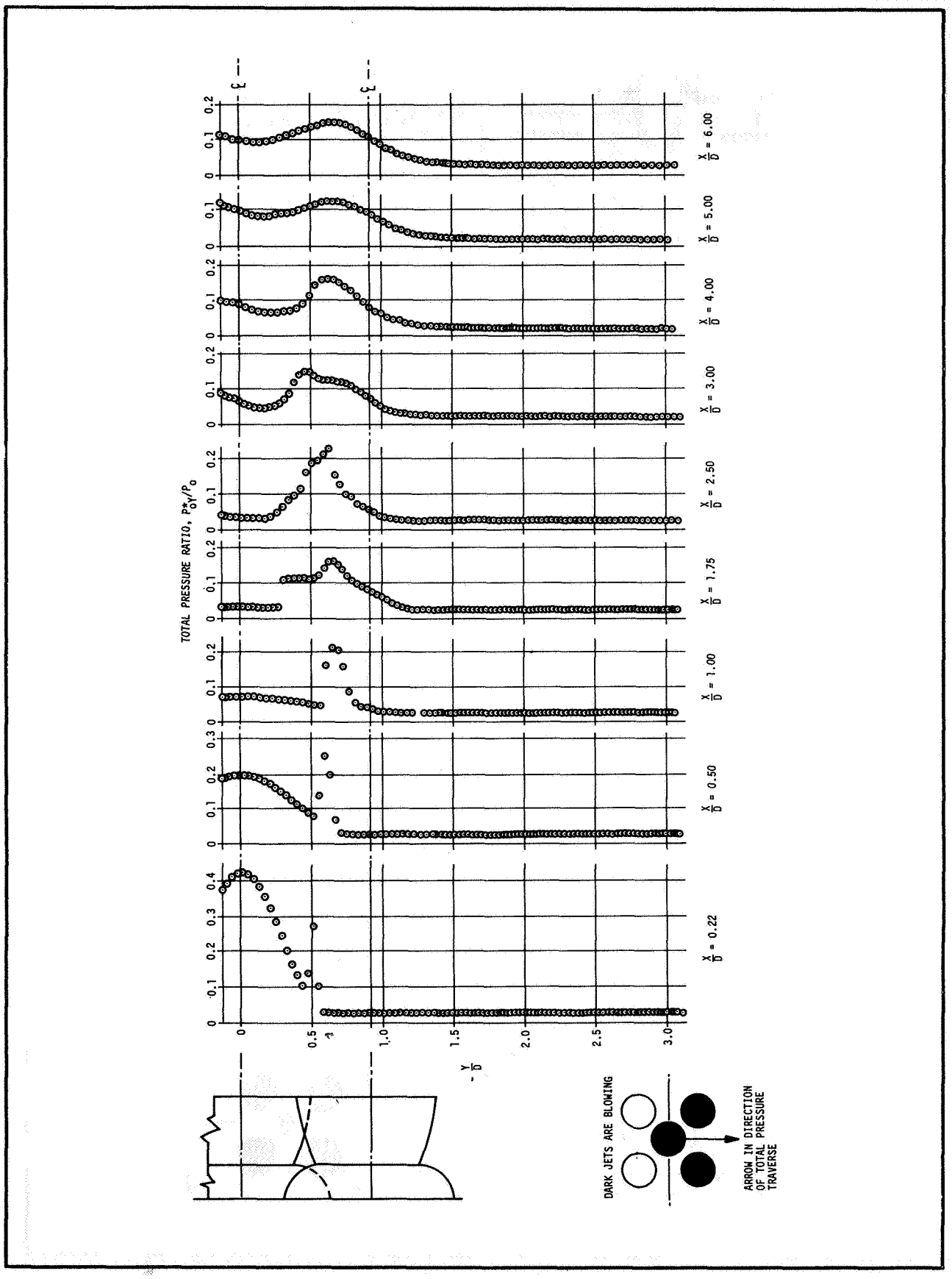

Figure 10c. PLUME TOTAL PRESSURE RATIOS FOR THREE JET CLUSTER IN TAJF COLD FLOW
P_o/P_a = 35.7, NOMINAL T_o = 500°R

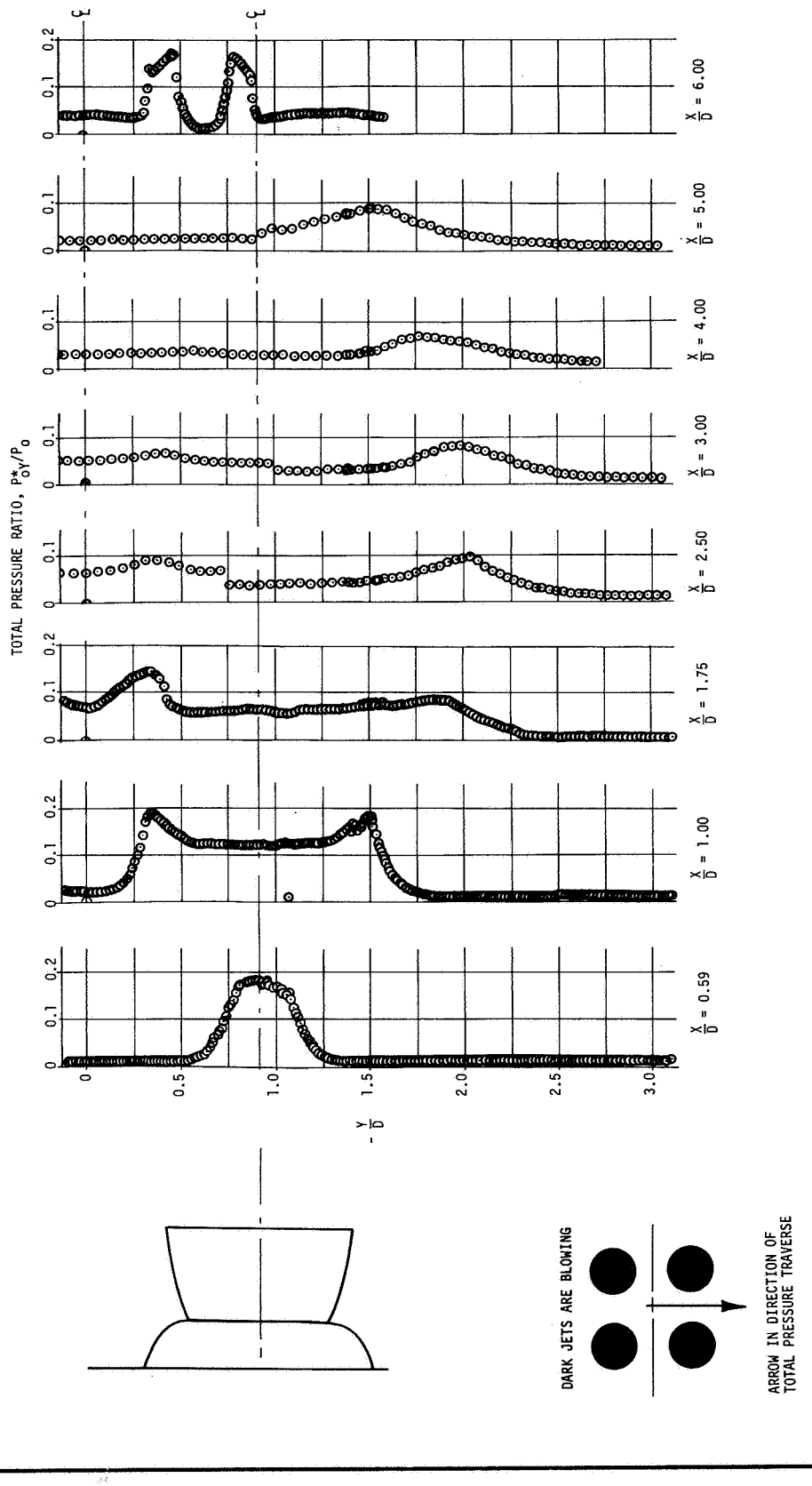

Figure 11a. PLUME TOTAL PRESSURE RATIOS FOR FOUR JET CLUSTER IN TAJF COLD FLOW
P_o/P_a = 105.2, NOMINAL T_o = 520°R

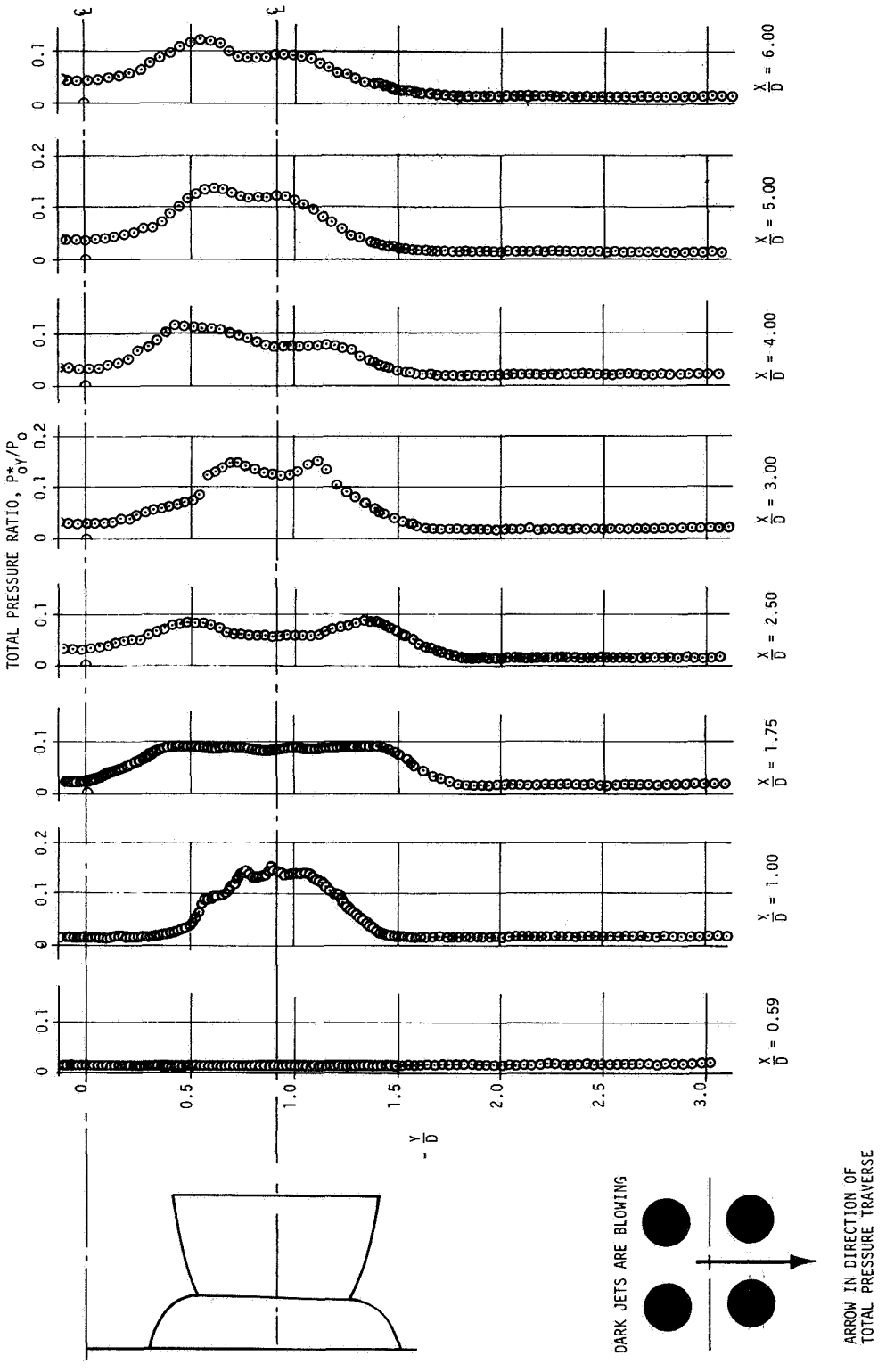

Figure 11b. PLUME TOTAL PRESSURE RATIOS FOR FOUR JET CLUSTER IN TAJF COLD FLOW
P_o/P_a = 63.5, NOMINAL T_o = 510°R

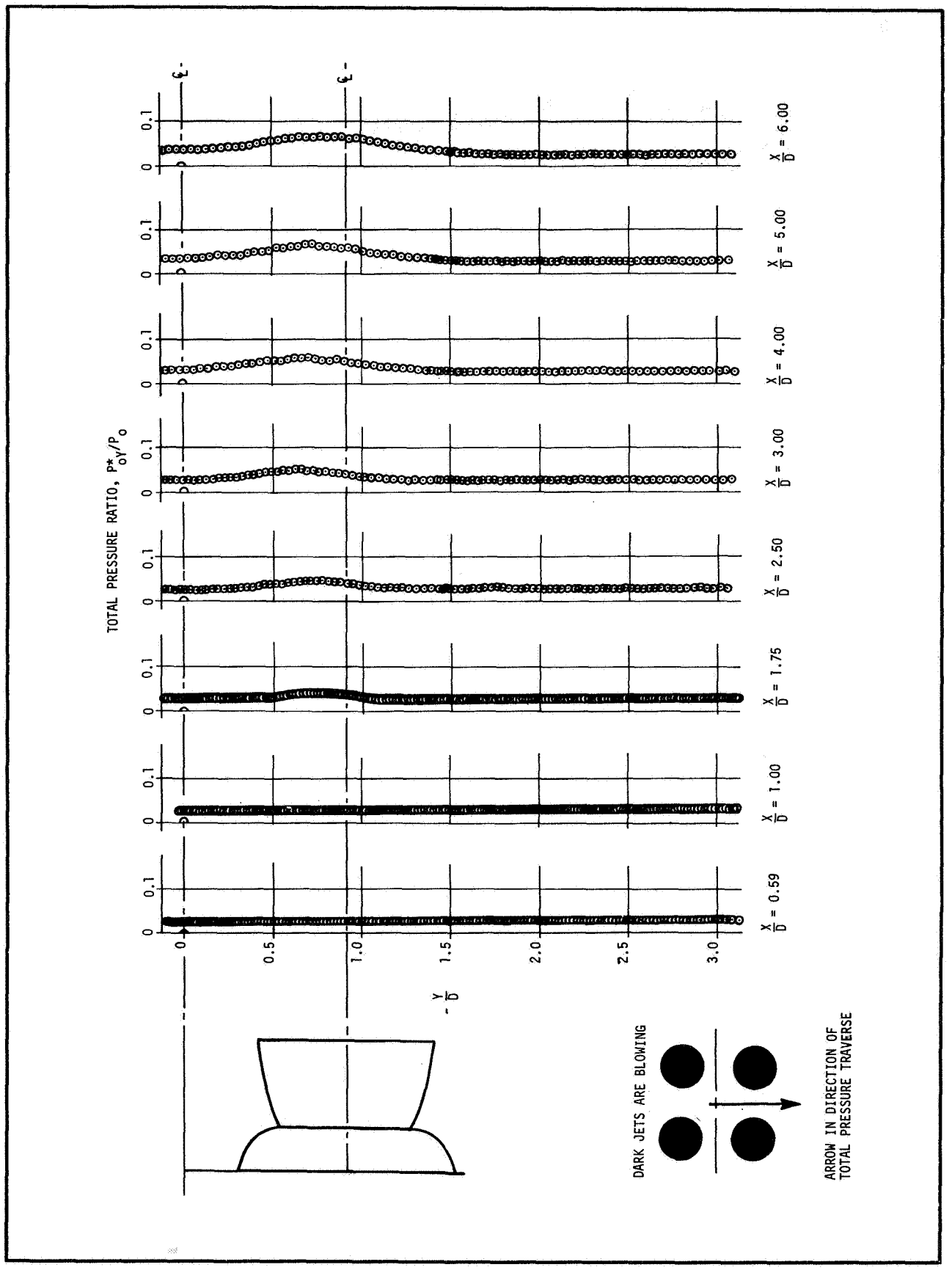

Figure 11c. PLUME TOTAL PRESSURE RATIOS FOR FOUR JET CLUSTER IN TAJF COLD FLOW
P_o/P_a = 35.7, NOMINAL T_o = 500°R

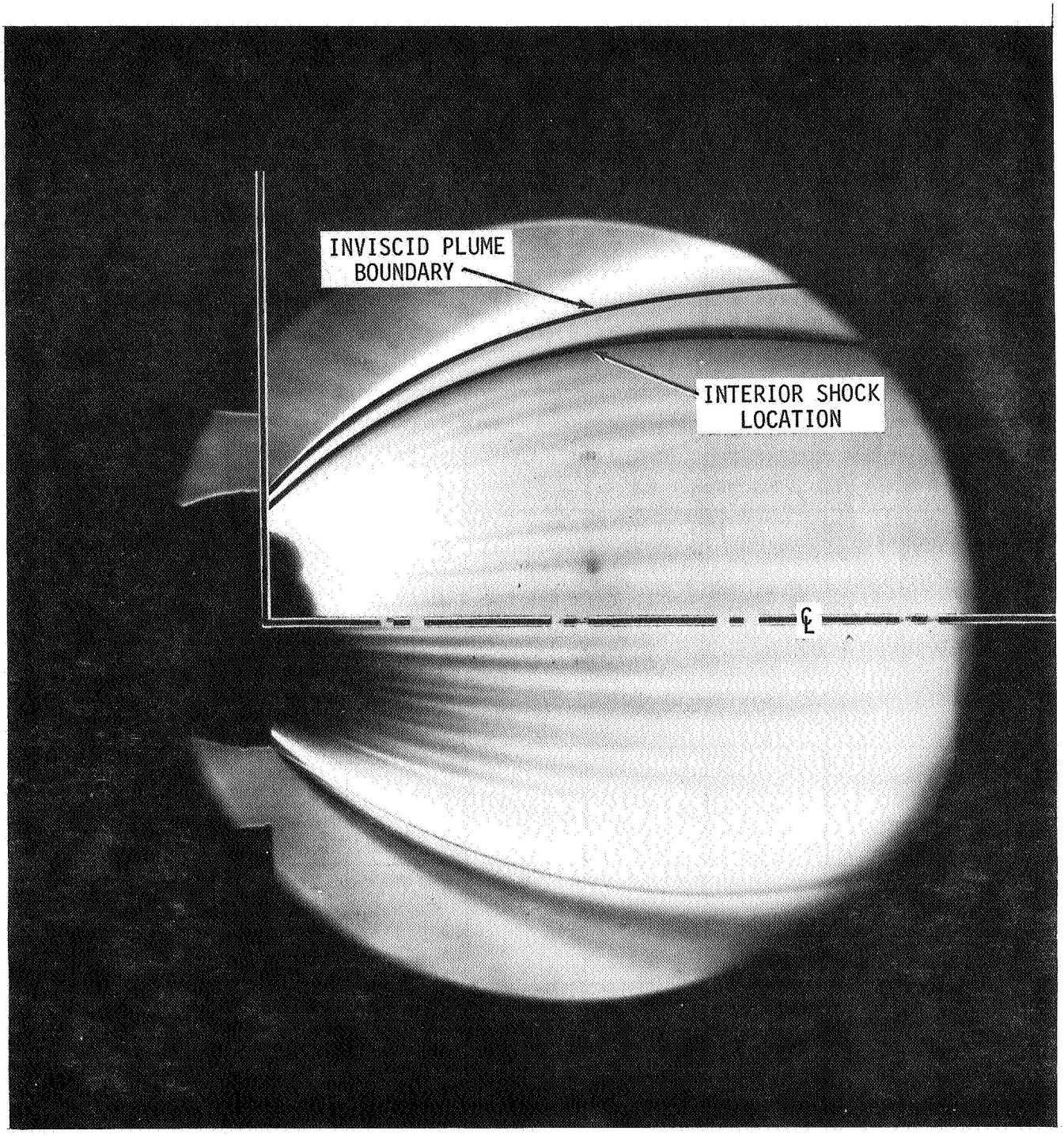

Figure 12. COMPARISON OF CHARACTERISTICS SOLUTION TO SINGLE JET FLOWFIELD (P_o = 1500 PSIG)

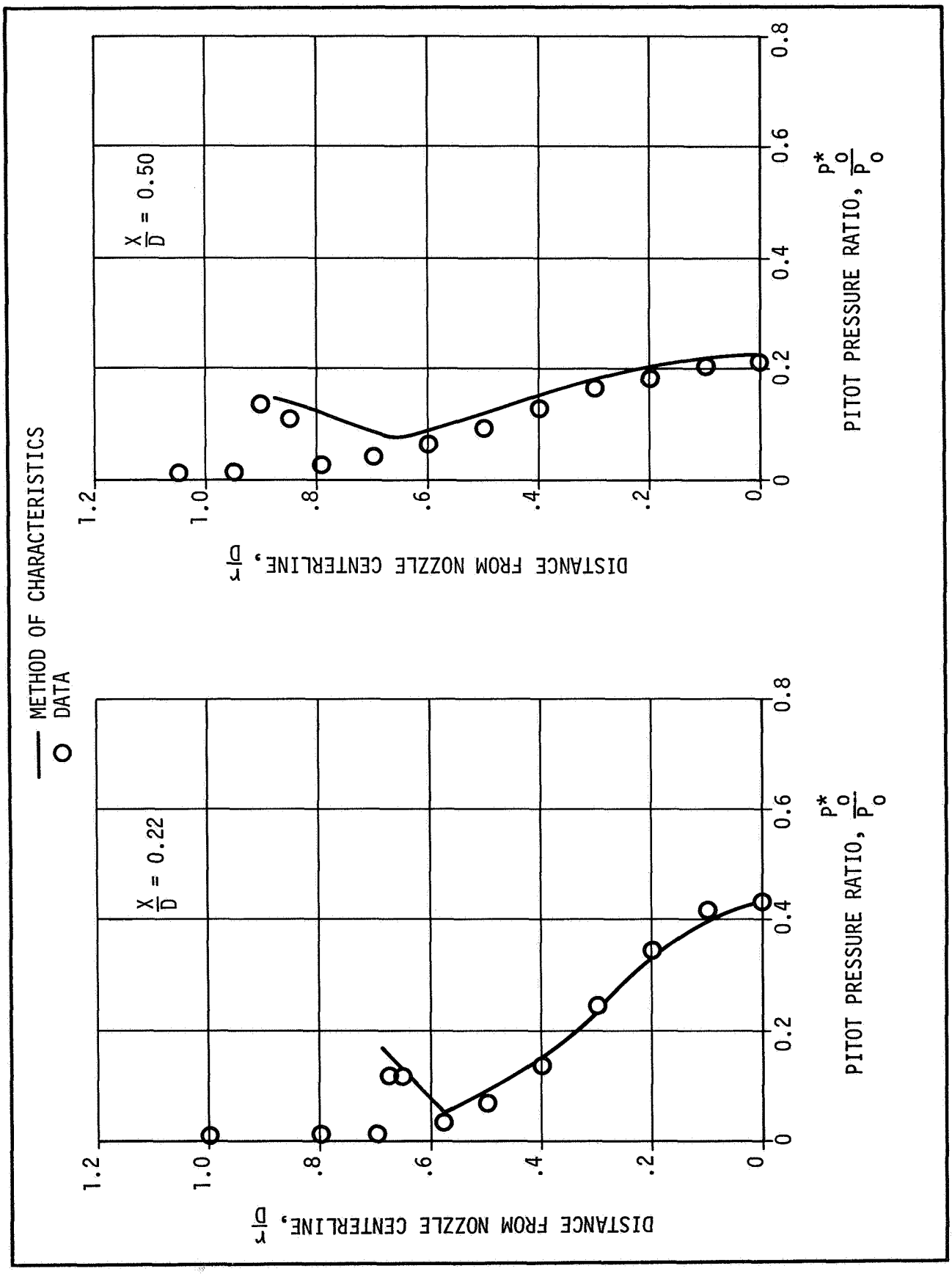

Figure 13. COMPARISON OF EXPERIMENTAL AND THEORETICAL PITOT PROFILES

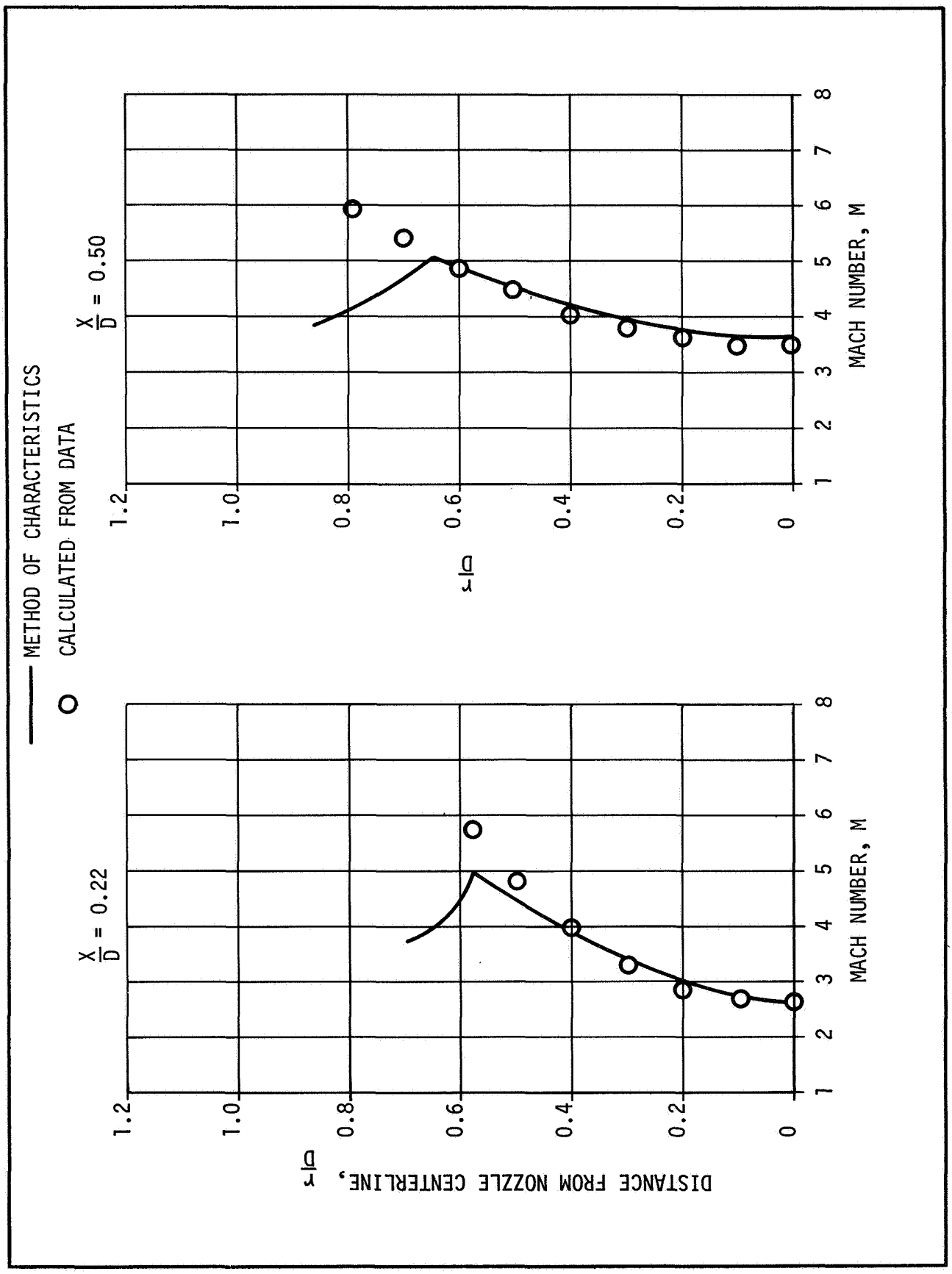

Figure 14. COMPARISON FOR CHARACTERISTICS SOLUTION AND ONE-DIMENSIONAL FLOW

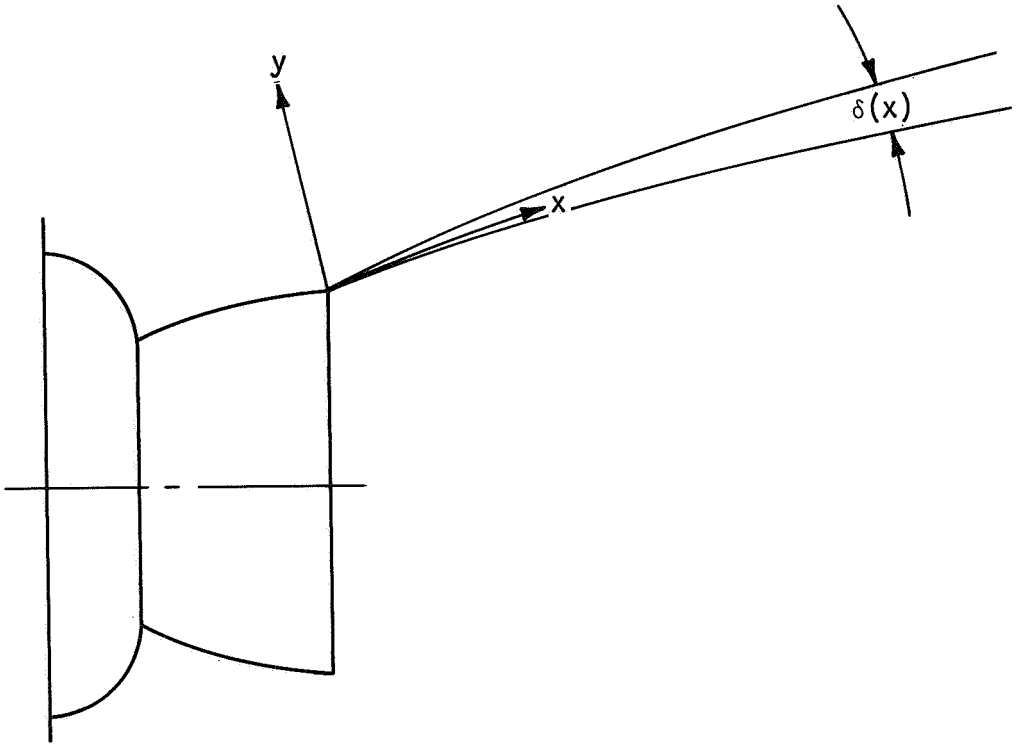

Figure 15. COORDINATE SYSTEM FOR ABRAMOVICH CORRELATION

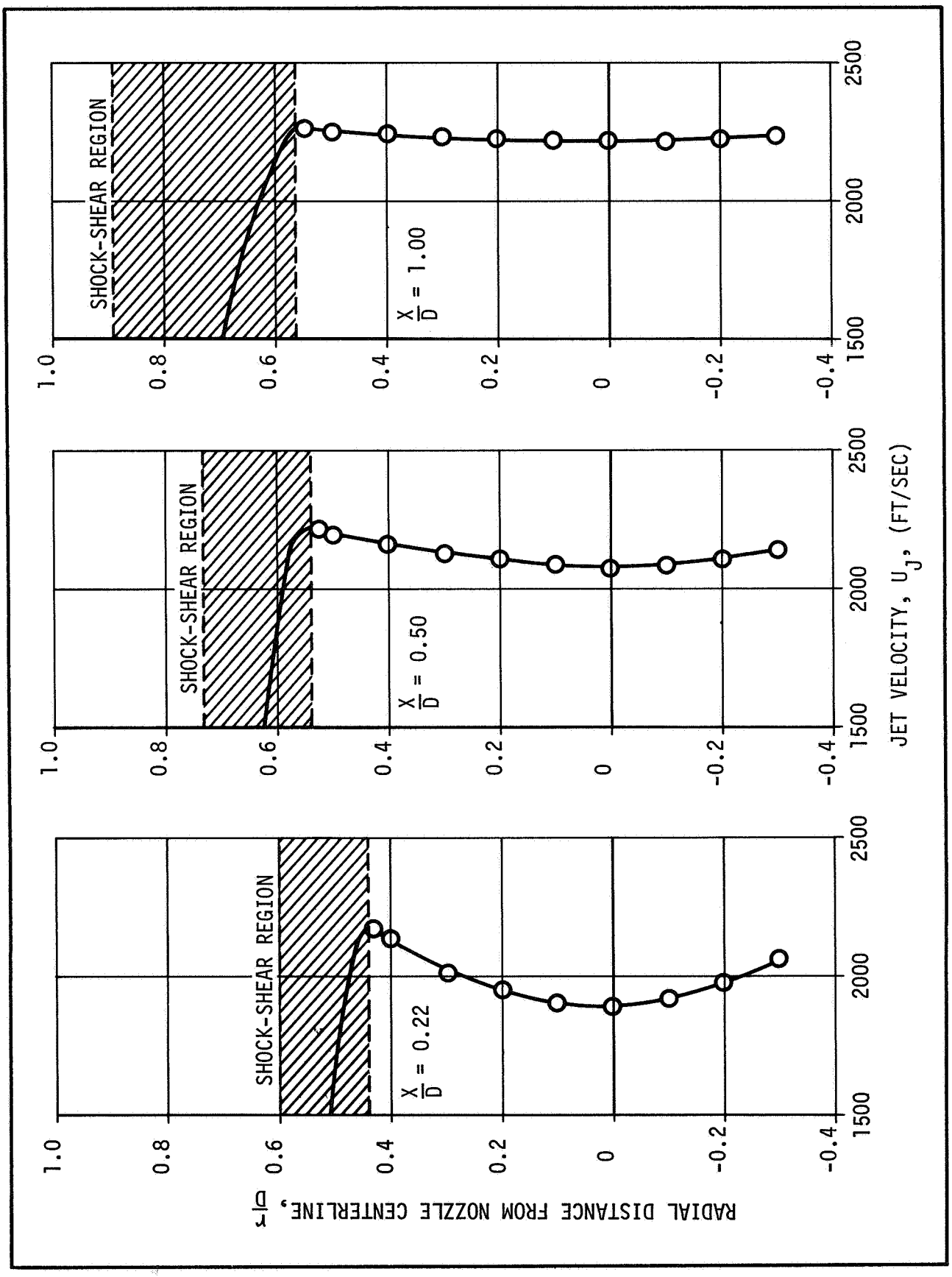

Figure 16. VARIATION OF JET VELOCITY FOR SATURN CLUSTER MODEL (P_o = 500 psig)

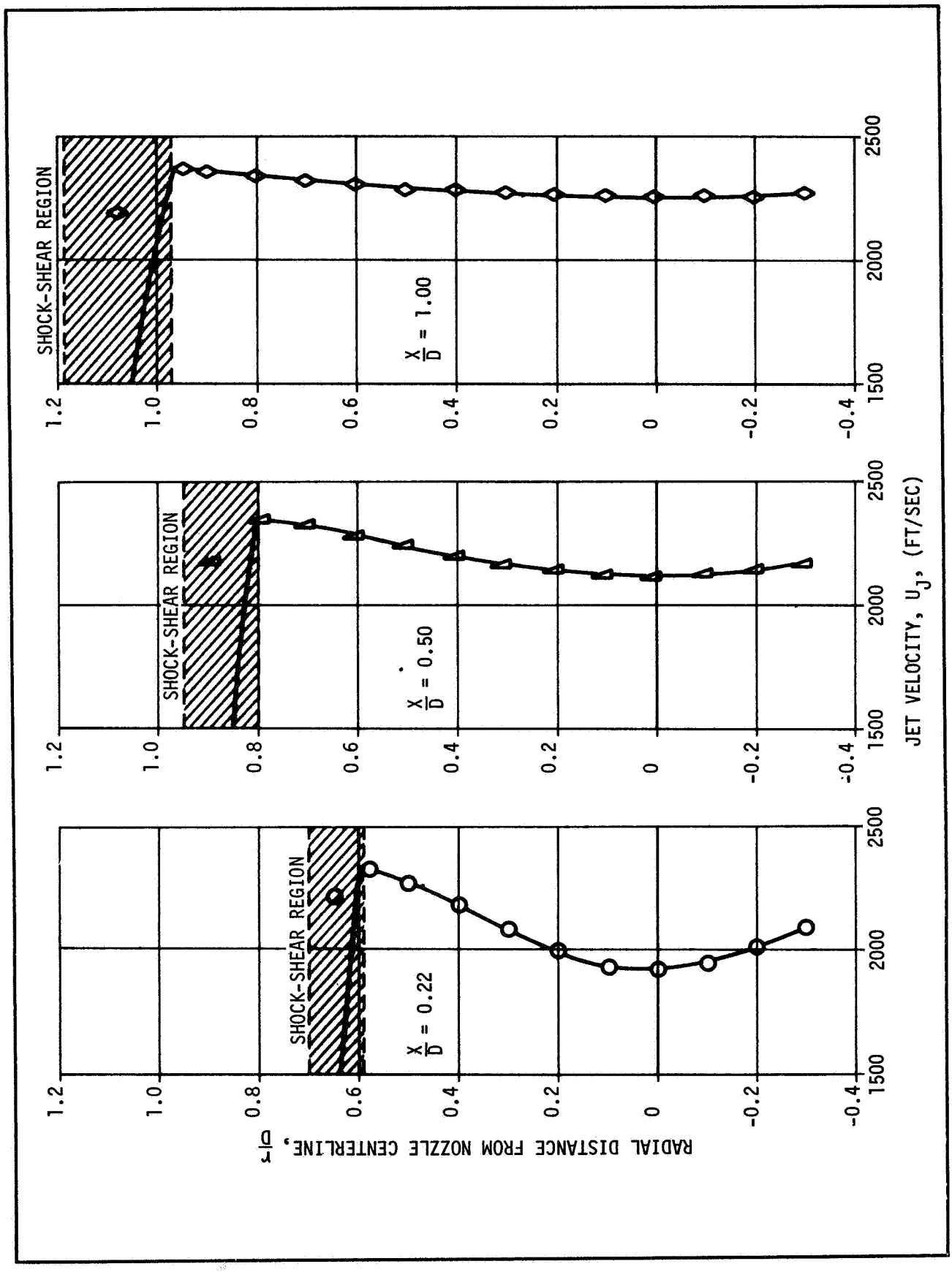

Figure 17. VARIATION OF JET VELOCITY FOR SATURN CLUSTER MODEL (P_o = 1500 psig)

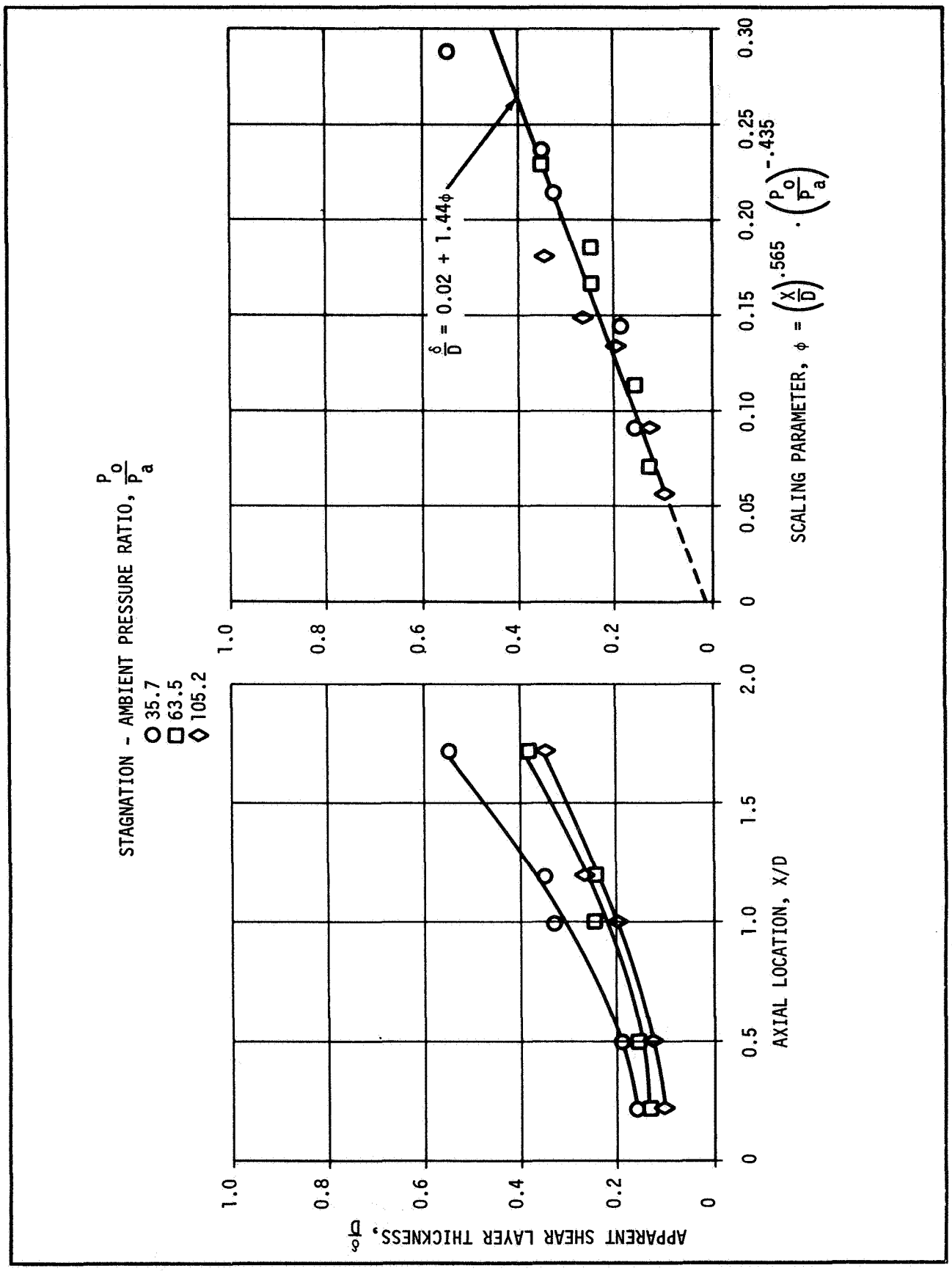

Figure 18. VARIATION OF SHOCK-SHEAR REGION THICKNESS NEAR THE EXIT PLANE OF THE NOZZLE

DISTRIBUTION

IITRI
10 West 35th Street
Chicago, Illinois 60616
ATTN: Mr. Damkevala
Dr. Clinch
Dr. Wilson
Dr. Dennen
Mr. Klugman
Col. Ferrell
Mr. Phillips
Mr. Norman
Mr. Wachowski
Mr. Cann
Dr. Sevin

Northrop-Huntsville
Technology Drive
Huntsville, Ala 35805
ATTN: Mr. Ryan
Mr. Bennett
Dr. Su
Mr. Barnett
Mr. Cikanek
Mr. Pooley
Mr. Tidmore

Colorado State University
Fort Collins, Colorado 80521
ATTN: Prof. Sandborn
Prof. Reiter

ESSA
National Bureau of Standards Bldg.
Boulder, Colorado 80521
ATTN: Mr. McGavin
Dr. B. Bean
Dr. G. Little

FAA No-10
800 Independence Ave. S.W.
Washington, D. C. 20590
ATTN: Dr. K. Power
Dr. J. Powers

NASA Headquarters
RAO, Mr. McGowan
RV-I, Mr. Cerreta
SAB, Mr. George
REI, Dr. Menzel
RV-2, Mr. Michel
RAA, Mr. Parkinson
RAP, Mr. Rekos
RRF, Mr. Schwartz

University of Oklahoma
College of Engineering
Norman, Oklahoma 73069
ATTN: Dean F. Black
Dr. Canfield

A&M College
Normal, Alabama 35762
ATTN: Prof. H. Foster
Mr. J. Shipman

University of Ala. Research Inst.
Technology Drive
Huntsville, Alabama 35805
ATTN: Dr. R. Hermann

MSFC
AST-U, Col. Mohlere
MS-T, Mr. Wiggins
S&E-EO-F, Mr. Attaya
S&E-COMP-RRV, Mr. J. Jones
S&E-ASTR-IA, Mr. Saunders
S&E-AERO-DIR, Dr. Geissler
S&E-AERO-T, Mr. Murphree
S&E-AERO-T, Mr. Cummings
S&E-AERO-Y, Mr. Vaughan
S&E-AERO-A, Mr. Dahm
S&E-AERO-A, Mr. Holderer
S&E-AERO-AU, Mr. Reed
S&E-AERO-AE, Mr. Heaman
S&E-AERO-AE, Mr. Simon
S&E-AERO-ATP, Mr. Huffaker
S&E-AERO-AF, Dr. Krause
S&E-AERO-AF, Mr. Funk
S&E-AERO-AF, Mr. Jayroe
S&E-AERO-AF, Mr. Ellner
S&E-AERO-AF, Mr. Stephens
S&E-AERO-AF, Mr. Kadrmas
S&E-AERO-AF, Mr. Thomison
S&E-AERO-AF, Mr. Jones (2)
S&E-AERO-AF, Mr. Kickelner
S&E-AERO-AF, Mr. Cliff

DISTRIBUTION (Concluded)

A&TS-MS-IL (8)
A&TS-MS-IP
S&E-ASTN-S, Mr. J. B. Sterett
S&E-CSE-I, Mr. Blacksone
S&E-CSE-ID, Mr. Roth
S&E-ASTR-A, Mr. von Pragenau
S&E-ASTR-A, Mr. Doss
S&E-ASTR-SE, Mr. Scofield
S&E-AERO-DDS, Mr. Keifling
S&E-ASTN-AD, Mr. Farrow
S&E-ASTN-ADL, Mr. Bullock
S&E-ASTN-PPA, Mr. Gross

The Boeing Company
Huntsville, Alabama
ATTN: Mr. Riley
Mr. McTigue
Mr. Tilden

North American-Rockwell
Holiday Office Center
Huntsville, Alabama
ATTN: Mr. Fleenor
Mr. Smith
Mr. Petrilla

Scientific and Technical Inf. Facility (25)
P. O. Box 33
College Park, Md. 20740